A probabilistic climate change assessment for Europe

Moghim, Sanaz; Teuling, Adriaan J.; Uijlenhoet, Remko

DOI
10.1002/joc.7604

Publication date
2022

Document Version
Final published version

Published in
International Journal of Climatology

Citation (APA)
Moghim, S., Teuling, A. J., & Uijlenhoet, R. (2022). A probabilistic climate change assessment for Europe. *International Journal of Climatology*, *42*(13), 6699-6715. https://doi.org/10.1002/joc.7604

Received: 26 March 2021 | Revised: 25 February 2022 | Accepted: 2 March 2022

DOI: 10.1002/joc.7604

RESEARCH ARTICLE

International Journal of Climatology RMetS

A probabilistic climate change assessment for Europe

Sanaz Moghim[1] | **Adriaan J. Teuling**[2] | **Remko Uijlenhoet**[2,3]

[1]Department of Civil Engineering, Sharif University of Technology, Tehran, Iran

[2]Hydrology and Quantitative Water Management Group, Wageningen University & Research, Wageningen, The Netherlands

[3]Department of Water Management, Delft University of Technology, Delft, The Netherlands

Correspondence
Sanaz Moghim, Department of Civil Engineering, Sharif University of Technology, Tehran, Iran.
Email: moghim@sharif.edu

Funding information
Wageningen University; University of East Anglia, Grant/Award Number: CMIP5

Abstract

Globally, the impacts of climate change can vary across different regions. This study uses a probability framework to evaluate recent historical (1976–2016) and near-future projected (until 2049) climate change across Europe using Climate Research Unit and ensemble climate model datasets (under RCPs 2.6 and 8.5). A historical assessment shows that although the east and west of the domain experienced the largest and smallest increase in temperature, changes in precipitation are not as smooth as temperature. Results indicate that the maximum changes between distributions of the variables (temperature and precipitation) mainly occur at extreme percentiles (e.g., 10% and 90%). A group analysis of four subregions of Europe, namely east (G1), north (G2), west/south (G3), and UK/Ireland (G4), shows that G1 and G4 are expected to have the largest increase in temperature and precipitation extremes, respectively. Although maximum increases in temperature in G3 and G4 occur at larger percentiles, G1 and G2 experience maximum increases at both large and small percentiles. The maximum increase of precipitation over the study domain, however, occurs mainly at larger extremes. To quantify changes in the distribution of projection (2020–2049) relative to the historical reference (1976–2005), two measures are defined, namely a change in occurrences (KS statistic) and intensities at different quantiles (Δ). Results confirm that the temperature distribution tends to shift to higher temperatures. Changes in distribution and extremes of precipitation are spatially variable. Furthermore, extremes are expected to be intensified under RCP 8.5. The quantile analysis and defined measures reveal changes in the entire probability distribution, reflecting possible climate changes in the future.

KEYWORDS

climate change, climate indicators, extreme weather events, impact assessment, probabilistic framework, quantile analysis

1 | INTRODUCTION

Many regions of the world have recently experienced the effects of climate change, albeit at different levels of severity. Climate change is a long-term change in the state of the climate, which can be defined by climatological variables such as air temperature and precipitation (IPCC, 2007). Climate change affects weather patterns and the hydrological cycle and can increase the frequency or intensity of extreme weather events such as heat waves and droughts (van der Wiel *et al*., 2017; Philip *et al*., 2018, 2019). The World Meteorological Organization (WMO) pointed out significant climate change impacts including wildfires, sea level rise, ice decline,

increase in heat content, and acidity of the ocean during 2015–2019, known as the warmest period on record (WMO, 2019). Many studies used different statistics of temperature and precipitation, such as changes in extreme values and number of hot/cold days/nights, to characterize climate change (e.g., Jeong *et al*., 2016; Wu *et al*., 2017; Solomon *et al*., 2007; Ye and Cohen, 2013; Cohen *et al*., 2015, among many others). Karl *et al*. (2008) showed that the number of hot days-nights has been increasing in most regions of North America, while the number of cold days-nights has been decreasing. To specify climate change and its impact, a proper set of measures and indicators is required, which can be defined based on climate change causes and effects (e.g., Climate Change Index, 2013). Sheikh *et al*. (2015) used indices based on temperature and precipitation observations to evaluate climate extremes over South Asia. Their results show that, generally, the warm and cold extremes are expected to increase and decrease, respectively. Similar changes are expected to occur in Australia (Alexander and Arblaster, 2017). Alexander and Arblaster (2017) used CMIP5 simulations to show an increase and decrease in the number of warm and cold temperature extremes by 2,100, respectively. In addition, their results indicated that the projections of the precipitation extremes tend to increase (e.g., more heavy rain and longer drought). Dosio (2017) analysed temperature and heat wave indices from Regional Climate Models (COordinated Regional climate Downscaling Experiment, CORDEX) over Africa. Results revealed an increase in temperature up to 6°C under RCP 8.5 in many parts of the continent, such as Northern Africa and the Sahara. Their findings indicated an increase not only in the number of the warm days and nights, but also in the length of the heat waves.

As in many other regions around the globe, warming of climate has accelerated in Europe (van der Schrier *et al*., 2013). Changes in mean temperature and precipitation have already led to changing patterns in evapotranspiration and streamflow across the continent (Teuling *et al*., 2019). van den Besselaar *et al*. (2013) analysed the trends in the frequency of 1-day and 5-day precipitation amounts with 5-, 10-, and 20-year return periods over north and south Europe. Their results showed that the frequency of those extreme events increased during 1951–2010. Climate change (e.g., temperature increase and precipitation decrease) is associated with extreme events, such as the severe flood and drought (Teuling, 2018), wildfires, and heat waves that occurred in southern Europe in 2017 (Kew *et al*., 2019). Lhotka *et al*. (2018) used E-OBS and regional climate model (RCM) data to evaluate heat waves and temperature changes in Central Europe. They stated that more severe heat waves are projected to occur in the future, while they found an overestimation of the heat waves' frequency simulated by the RCM at spatial resolution of 25 and 50 km. Although models can confirm that global warming increases extreme weather events, they are unable to correctly represent main characteristics (e.g., frequency and intensity) of the events (Min *et al*., 2013; Sippel *et al*., 2016; Kew *et al*., 2019).

Assessment of climate change includes accounting for uncertainties. One of the main frameworks to consider uncertainties and provide a wide range of changes is the probabilistic approach (Jahangir and Moghim, 2019; Moghim, 2021). Watterson (2008) used pattern scaling to estimate projected probability distribution functions (PDFs) of temperature and precipitation in Australia under the A1B scenario. Results showed a possible range of regional warming based on constructed PDFs in southern Australia. In addition, their findings indicated that the projected winter rainfall in the centre of Australia varies from a large decrease to a modest increase. Dessai *et al*. (2005) used a probabilistic energy balance model to assess various uncertainties in climate change probabilities. Their results showed that uncertainties in emission scenarios and climate sensitivity are important at the 9fifth and fifth percentiles of the temperature distributions, respectively. However, the impact of uncertainties in emissions, climate sensitivity, carbon cycle, ocean mixing, and aerosol forcing on percentiles of precipitation distributions varies in time and location (Dessai *et al*., 2005). The impact of climate change on extreme hydrometeorological values (small and large quantiles of the distribution) is more remarkable than average ones in many regions (e.g., Lausier and Jain, 2018, Moghim, 2018, among many others). Different quantile analysis methods (e.g., the quantile regression method) can evaluate changes not only in the mean but also in other percentiles of the distribution (Koenker, 2005). Dhakal and Tharu (2018) used a linear quantile regression approach to evaluate the effect of North Atlantic tropical cyclones on extreme precipitation across 107 sites in the southeastern United States. Their results showed an increasing trend of upper quantiles in most sites, which can be due to the tropical cyclones. This extreme analysis is invaluable for water resources and disaster/crisis management. Richardson *et al*. (2020) used weather patterns (WPs) and the upper end of the precipitation distribution to define flood events due to extreme precipitation in the UK. The relationship between WP and extreme precipitation is used for flood forecasting, which is a valuable resource for managers to decrease the risk of flood events. van der Wiel *et al*. (2017) defined extreme precipitation and examined the impact of anthropogenic forcing on the likelihood of extreme precipitation in the

Gulf Coast region. In addition, they assessed flood events in southern Louisiana. Their results show an increase in extreme precipitation since 1900. Ganguli and Ganguly (2016) used the persistence probability of drought to evaluate the spatial patterns of mean and extreme droughts over the Contiguous United States. Their results showed that the spatial coverage of the recent extreme drought (after 2010) is larger than that of the previous droughts (e.g., the 1930s and 1950s), while the persistence of the drought has been stationary during the last half of the century.

Although many studies attempt to link climate change to an increase in the occurrence and severity of hydrological extremes, the limited number of recorded occurrences increases the uncertainty of the analysis. This asks for a more robust assessment (Stott, 2016). Furthermore, many studies are unable to demonstrate a clear trend in climate change signals due to a lack of proper climate change indicators (Kossin, 2018; Blöschl *et al*., 2019; Moon *et al*., 2019). Inconsistent results of climatic signals in Europe and many other regions indicate a necessity for more studies and analyses of climate change impacts. In addition, although evidence can clearly point out some signs of global warming, such as a dramatic decline in Arctic ice mass (Witze, 2019), climate change effects are not easily detectable in all regions. To elucidate climate change signals, a proper set of statistical measures is required. The skill of such measures to highlight climate change may vary in different locations. Here, we aim to analyse recently and projected climate change across Europe using a probabilistic framework, with a particular focus on changes in extremes of (air) temperature and precipitation (as the two main indicators of the climate change).

2 | DATASETS

To assess climate change in Europe, this study evaluates the historical changes using CRU (Climate Research Unit) data and projections of future climate change using climate models.

2.1 | Climate research unit (CRU) gridded data

CRU product is one of the most common datasets that are widely used in hydro-climatic studies (e.g., Moghim and Bras, 2017, 2019; Li *et al*., 2010; Sheffield *et al*., 2006, among many others). This gridded dataset is prepared by the School of Environmental Sciences and the Tyndall Centre at the University of the East Anglia, United Kingdom (data are publicly available at http://www.cru.uea.ac.uk/data). This long record of data that is compiled from global weather stations is validated by climatologies. The dataset is in 0.5° monthly resolution from 1901 to 2016 (Harris *et al*., 2014). The CRU temperature and precipitation records (the two main climatological variables of interest) are used for the historical overview of climate change. To assess the changes, these monthly data are divided into two periods, namely 1976–2005 (Per1) and 2006–2016 (Per2), in order to analyse recent changes from the observational records. The difference of the domain average of the variables (temperature and precipitation) between two periods and the empirical cumulative distribution functions (ECDF) of the variables are used to evaluate historical climate change.

2.2 | Ensemble climate model projections, coupled model Intercomparison project phase 5 (CMIP5)

General circulation models (GCMs) are the advanced numerical models that simulate physical processes and various feedbacks of the global climate system under different scenarios (Nakicenovic *et al*., 2000; Moss *et al*., 2008; Moss, 2010). These scenarios are defined by the Intergovernmental Panel on Climate Change (IPCC) based on greenhouse gas (GHG) concentration pathways. GCMs are the main tool to project climate changes and study the long-term effects of climate change. The Canadian Centre for climate modelling and analysis provided Coupled Model Intercomparison Project Phase 5 (CMIP5)-gridded data. In addition, this Centre used 29 models of the CMIP5 to provide an ensemble product at 1° monthly resolution (data are publicly available at http://climate-scenarios.canada.ca). We found this ensemble product to be more consistent with the observation (smaller error in temperature and precipitation relative to the CRU data) over the study domain compared to individual GCMs, thus this study uses this ensemble climate data (hereafter called ensemble) under two different RCPs (Representative Concentration Pathways), namely RCP 2.6 and RCP 8.5 for climate change projections. These RCPs show pathways of the radiative forcing up to 2,100. RCP 2.6 comprises storylines to limit global mean temperature rise to 2°C and represents the best-case scenario (Rapid Emissions Reductions); RCP 8.5, on the other hand, accounts for the highest GHG emissions and represents the worst-case scenario (Continued Emissions Increases). Thus, future projections under RCP 2.6 and RCP 8.5 cover the range of projected changes (minimum and maximum values, respectively). To assess projections of future climate change, the model outputs (namely temperature and precipitation) under historical, RCP 2.6,

and RCP 8.5 scenarios are used (data are publicly available at http://climate-scenarios.canada.ca). Monthly temperature and precipitation data are divided into two 30-year periods, namely the baseline (1976–2005) and the projection (2020–2049).

3 | METHODOLOGY

The perceived level of climate change depends on how changes are assessed. A proper and comprehensive analysis can clarify changes. This study uses (air) temperature and precipitation as two important hydroclimatological variables to assess climate change over Europe, for different subdomains, and for each individual pixel. Although climate change can affect the first moment (mean) of the variables, its effect varies at different percentiles of the probability distributions of monthly temperature and precipitation. In addition, the impact of climate change on the distribution at different quantiles varies between locations. To quantify distribution changes, differences between monthly temperature and precipitation distributions of the two periods at various percentiles, comprising the 10th, 50th, and 90th percentile (median and extremes), are calculated.

Furthermore, the larger and smaller quantiles of the variables (extremes) are evaluated probabilistically to include uncertainty of the results. To further evaluate distribution changes, probabilities of the values corresponding to the specific quantiles in period 1 are obtained from distributions of period 2 for each pixel (Figure 1a).

Changes in the probability at different quantiles can also translate to the actual values of the hydroclimatological variables. To illustrate the incremental changes in the variables, the difference between two distributions of periods 2 and 1 at specific quantiles is calculated (Δ, see red solid line in Figure 1b).

Climate studies can refer to the past and future; For instance, historical evidence and analysis to show that climate has been changing or climate change projections to show possible changes in the future using climate models under different scenarios. This study uses CRU data (see Section 2.1) for Part 1 (historical assessment) and ensemble climate model projections (see Section 2.2) under two scenarios (RCP 2.6 and RCP 8.5) for Part 2 (projection). For the model-observation comparisons, data are bilinearly regridded to a common grid. To estimate historical climate change, we calculate average changes in precipitation and temperature in Per2 (2006–2016) relative to Per1 (1976–2005). To consider uncertainties and a different length of Per1 compared to Per2, for a 95% confidence interval, we use the bootstrap method and randomly resample 10 years from 30 years of Per1 (1976–2005) with 5,000 replicates. The average differences between each set of 10-year sampled data (average temperature and precipitation) in Per1 and Per2 at the 95% confidence level are calculated and presented for each pixel. Similarly, for an estimate of projected changes in temperature and precipitation, we randomly sample sets of 10 years from the projection (2020–2049) and baseline (1976–2005) periods under two scenarios (RCP 2.6 and RCP 8.5). The average differences between sets of temperature and precipitation in two periods at the 95% confidence level are calculated and presented for all pixels. Similarly, to assess seasonal changes, the average differences between random samples of seasonal temperature and precipitation in the two periods (baseline and projection) are obtained. Although the average changes of the variables in period 2 and projection relative to the baseline over the entire domain can provide an integrated view of the observed or projected climate change, average changes cannot illustrate large increases or decreases that occur over different subdomains. Thus, Europe is divided into different subregions (groups of countries) for a

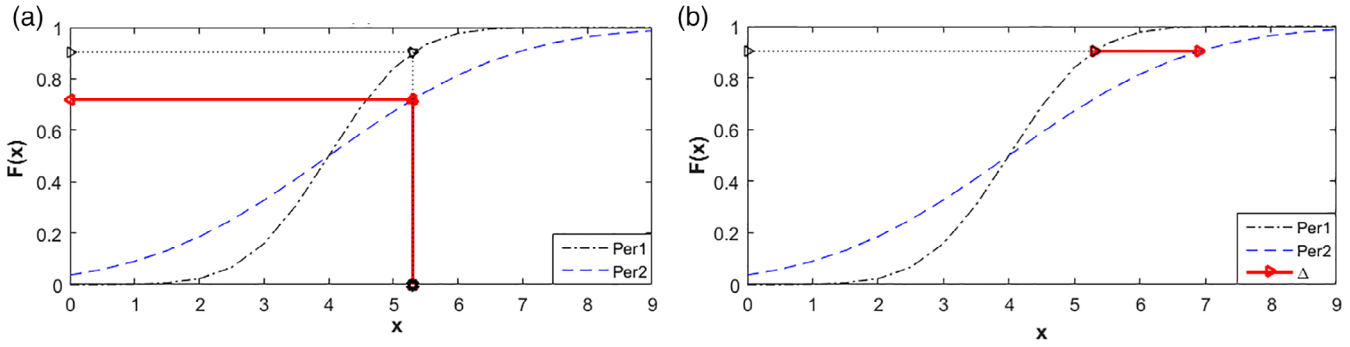

FIGURE 1 Illustration of the distribution assessment. (a) Based on the probability changes and (b) based on the actual values at specific quantiles [Colour figure can be viewed at wileyonlinelibrary.com]

cluster analysis. This analysis can assess climatic changes at an appropriate scale and point out dominant changes in each subregion, which indicates that people in different regions should be prepared for different types of possible changes in the future. Indeed, different scenarios of climate change need to be considered to assess potential damages and losses, based on a plausible range of future outcomes. To analyse projected quantiles, changes in the probability distributions of the ensemble data (temperature and precipitation) for the projection (2020–2049) relative to the baseline (1976–2005) period are evaluated. In addition, due to different projected changes in distributions of the variables (temperature and precipitation) within the domain, we calculate the incremental distance between the projected and historical distributions at different percentiles for each subregion with a significance level of 0.05. To construct empirical CDFs for the baseline and the projection, we use 30 years of monthly ensemble data (temperature and precipitation) from future (2020–2049) and historical (1976–2005) periods, respectively. The Δ (incremental distance) between CDFs of the two periods (projection and baseline) is calculated at median and extremes (i.e., 50th, 10th, and 90th percentile). To evaluate possible changes in extremes, empirical CDFs of monthly temperature and precipitation are constructed for Per1 (1976–2005) at each pixel ($ECDF_1$). To establish $ECDF_1$, we randomly select 10 years from Per1 (1976–2005) for 5,000 times. To find extreme values in Per1, the 10th and 90th percentile of the constructed $ECDF_1$ for the temperature and precipitation are obtained ($T_{10\%\ of\ Per1}$ and $T_{90\%\ of\ Per1}$ for temperature; $P_{10\%\ of\ Per1}$ and $P_{90\%\ of\ Per1}$ for precipitation). Then, we calculate the probability that each pixel in Per2 (2006–2016) has average monthly temperature or precipitation smaller/larger than the extreme percentiles (10th/90th) of the $ECDF_1$ of the corresponding variables (hereafter called Pr_{ext}). In other words, the Pr_{ext} is calculated as the probability of having average monthly temperature or precipitation in Per2 smaller than $T_{10\%\ of\ Per1}$/$P_{10\%\ of\ Per1}$ or larger than $T_{90\%\ of\ Per1}$/$P_{90\%\ of\ Per1}$ for temperature/precipitation. This assessment can help identify hazards of the extreme events in different subregions. Changes at large and small quantiles can illustrate the tendency of the regions to have more rain (floods) and less rain (droughts), which is useful for water resources management plans and impact assessment. For instance, larger changes in smaller/larger quantiles can be considered for drought management/flood control.

Climate studies need measures and indicators to illustrate and monitor changes. Since the future is uncertain, probabilistic measures are appropriate indicators of climate change. Thus, this study focuses on two such probabilistic measures, the KS statistic and Δ, which can reflect changes in the distribution of the projection (future) relative to the historical period. The two largest "vertical" (KS) and "horizontal" (Δ) differences between two distributions highlight the distribution changes and extremes. The KS (Kolmogorov–Smirnov) test statistic, which can be interpreted as a change in occurrences, is the largest distance between two cumulative distribution functions (CDFs) measured along the probability axis, defined as

$$\mathrm{KS} = \max_x \left\{ F_{\mathrm{Proj}}(x) - F_{\mathrm{His}}(x) \right\} \quad (1)$$

In this study, F_{Proj} and F_{His} are empirical CDFs of the variable x (monthly temperature or precipitation) in the projection and historical periods, respectively (see Figure 1a). Similar to $ECDF_1$, empirical CDFs for projection are constructed from 30 years (2020–2049) of monthly ensemble temperature and precipitation ($ECDF_{Proj}$). The KS measure has been used to show the performance skill of a model in a probability framework (Moghim and Bras, 2017, 2019). The second measure, Δ (see Figure 1b), can be interpreted as a change in intensities (value associated with a given percentile). To obtain Δ, the difference between values of the variables (temperature and precipitation) in two distributions (historical and projected) are calculated at median and extremes (i.e., 50%, 10%, and 90%). The increment Δ can be used to correct the biases of the climate models (Moghim *et al*., 2016). To evaluate the variability of the changes at different percentiles, mean (μ) and standard deviation (σ) of the Δ are calculated.

The defined indicators, which reflect changes in the entire distribution, are employed to highlight the effects of climate change (in terms of temperature and precipitation) over different regions. A significance level of 0.05 ($\alpha = 0.05$) is used for the results in this paper that are statistically significant.

4 | ASSESSMENT OF HISTORICAL CLIMATE CHANGE IN THE 20TH CENTURY

The historical change of temperature and precipitation based on average differences between sampled 10-year sets of data in Per2 (2006–2016) and Per1 (1976–2005) is shown in Figure 2 (first row). Results indicate that all regions have experienced an increase in annual mean temperature since Per1. This increase is most prominent over the eastern part of Europe (the maximum and minimum increases are found in Ukraine and Ireland, respectively). Results show that the spatial change (increase

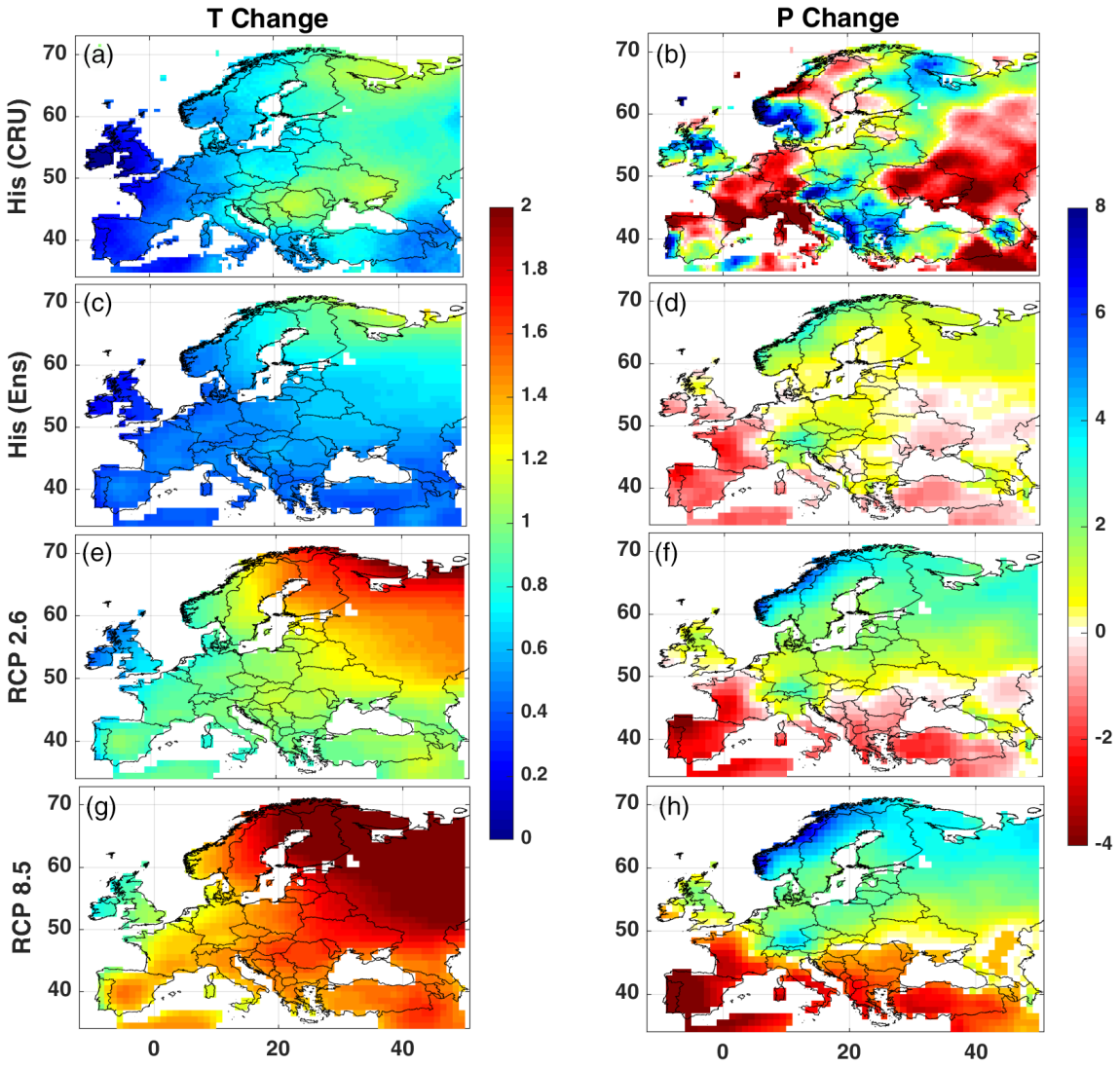

FIGURE 2 Spatial changes in the observed and projected temperature (°C) in the left column and precipitation (mm·Mon^{-1}) in the right column. Spatial average changes between two periods (Per2: 2006–2016 and Per1: 1976–2005) from CRU [his (CRU) in first row] and the ensemble model [his (Ens) in second row]. Spatial average changes between two periods (projection: 2020–2049 and baseline: 1976–2005) from ensemble model under RCP 2.6 (third row) and RCP 8.5 (fourth row) [Colour figure can be viewed at wileyonlinelibrary.com]

and decrease) of precipitation is more variable than temperature. For instance, the maximum increase and decrease of precipitation occurs at close pixels. The spatial variability of changes in precipitation, including a decrease in average precipitation under climate change in parts of Southern Europe, is consistent with the results obtained by van den Besselaar *et al.* (2013), Casanueva *et al.* (2014), and Jacob *et al.* (2014). The maximum increase and decrease of annual mean precipitation occurred in Norway and Italy, respectively. Note that results presented for all pixels are in the 95% confidence level.

Although the domain-average analysis showed that temperature and precipitation have changed, the average assessment is not able to highlight significant changes in different regions. Indeed, the impact of climate change can be more noticeable on extremes (maximum and minimum). To assess extreme changes, the exceedance probability of monthly air temperature and precipitation in Per2 (2006–2016) at the 10th and 90th percentile of $ECDF_1$ ($ECDF$ for Per1) is calculated (Pr_{ext}) for each pixel (Figure 3).

Figure 3 shows the probability in each pixel that average monthly temperature or precipitation in Per2 (2006–2016) is smaller/larger than the extreme percentiles (10th/90th) of the $ECDF_1$ of the corresponding variables. Results show an increase in occurrence of cold temperature extremes (below percentile 10) in some northern parts of the study domain (see blue colour in Figure 3a). In other words, these regions tend to have smaller

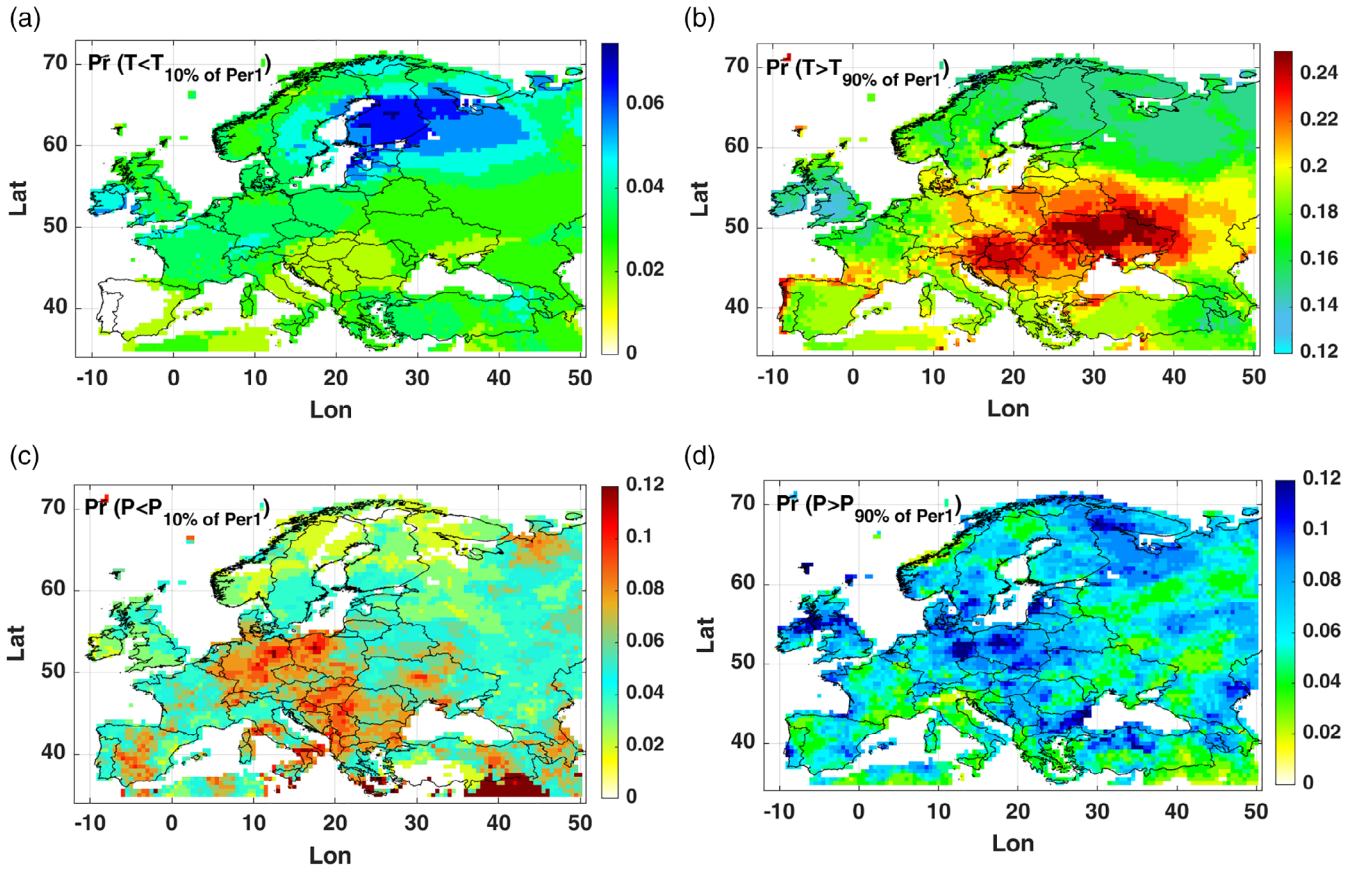

FIGURE 3 Changes in probability of observed extremes. Extremes are calculated for Per2 relative to Per1; probability of average monthly (a) temperature in Per2 being smaller than 10th percentile of temperature in Per1, (b) temperature in Per2 larger than 90th percentile of temperature in Per1, (c) precipitation in Per2 smaller than 10th percentile of precipitation in Per1, and (d) precipitation in Per2 larger than 90th percentile of precipitation in Per1 (Per1: 1976–2005 and Per2: 2006–2016) [Colour figure can be viewed at wileyonlinelibrary.com]

minimum temperature in 2006–2016 compared to their baseline period (1976–2005). The central part of the domain has experienced a greater increase in extreme temperature, above 90% (see red colour in Figure 3b). The reddish/bluish colour in the second row of Figure 3 (Figure 3c,d) shows regions that are more likely to have extremes (minimum/maximum) in precipitation.

5 | ASSESSMENT OF CLIMATE CHANGE PROJECTIONS

The analysis of the CRU-gridded data (observations) confirms the variation trends of temperature and precipitation. The second row in Figure 2 shows the average differences of sampled 10-year sets of temperature and precipitation of the ensemble product in Per2 (2006–2016) and Per1 (1976–2005). Results show that the model underestimates temperature and precipitation changes in almost all pixels, which is consistent with the IPCC assessments. Collins *et al.* (2013) claimed that although model averages can be considered as best estimates, the averages can lead to underestimations. The third and fourth rows of Figure 2 show the projected average changes in mean annual temperature and precipitation in (2020–2049) relative to the baseline (1976–2005) under two scenarios (RCP 2.6 and RCP 8.5). Results confirm that temperature tends to increase in the eastern part of Europe, particularly in the northeast. The pattern of precipitation changes is more complex and uncertain than temperature due to the complexity of the precipitation process. Figure 2e,g show that all regions are expected to experience a temperature rise, with the largest increase over the northeast of Europe. For precipitation, the maximum change is almost 10 times as large as the average spatial change, which confirms larger variability in precipitation than temperature. RCP8.5 shows an intensification of the spatial pattern of changes in average precipitation and temperature. This leads to higher maximum/minimum changes in average temperature and a rise in maximum increase/decrease in average precipitation, compared to RCP2.6 (third and fourth rows of

Figure 2). Note that results presented for all pixels are at the 95% confidence level.

Annual average changes can hide a balance between increases in winter and decreases in summer. Indeed, the characteristics of climate change can have significant seasonal dependencies. Figure 4 shows seasonal changes of the ensemble temperature and precipitation between projection and baseline periods under two scenarios.

Results confirm that the pattern of changes in each season is different. The maximum changes in seasonal temperature occur in winter mainly in the northeast to north of the domain (Russia to Finland). Although the pattern of temperature changes in winter, spring, and fall follows the pattern of the mean annual changes (Figure 2), the pattern of increase in summer temperature is almost uniform over the domain under both scenarios. In RCP 8.5, the large increase in temperature extends from the northeast to the north and to the centre in winter and spring, while most of the pixels experience a large increase in temperature in summer and fall. Although the temperature of most pixels increases about 2° in summer, the centre of the domain (e.g., Romania and Serbia) experiences the largest increase of about 2.5° in RCP 8.5. For precipitation, most pixels in the north/south of the domain experience an increase/decrease in precipitation, while a marked contrast between increases and decreases is evident in summer and fall. In general, 85%, 80%, 53%, and 77% of the domain pixels experience an increase in precipitation in winter, spring, summer, and fall, respectively. Note that results presented for all pixels are at the 95% confidence level. Changes (both increase and decrease) in seasonal precipitation are larger under RCP 8.5, which can indicate that we need to expect more extreme hydrological events like floods and droughts in the future.

The analysis of the CRU-gridded temperature and precipitation (observations) confirms that climate change affects various percentiles of the distributions differently. To analyse projected quantiles, the Δ (see Figure 1b) between CDFs of the 2020–2049 and 1976–2005 (projection and baseline) at different percentiles are calculated. The maximum difference between distributions of the two periods at those percentiles occurs at 10% and 90% for temperature and precipitation. Therefore, we use

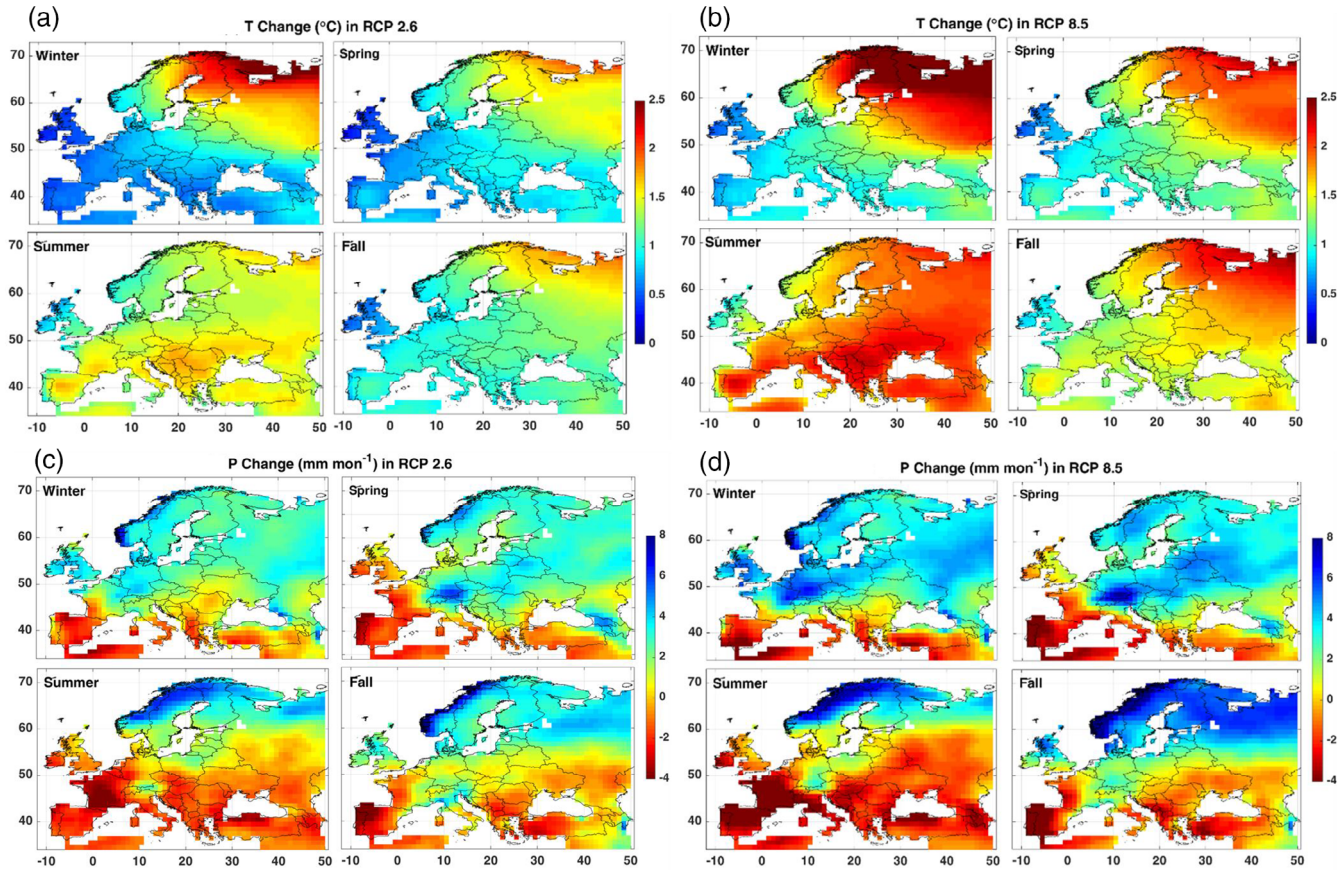

FIGURE 4 Average seasonal changes between two periods (projection: 2020–2049 and baseline: 1976–2005) from ensemble data. Spatial average changes for (a) temperature (T) under RCP 2.6, (b) temperature (T) under RCP 8.5, (c) precipitation (P) under RCP 2.6, and (d) precipitation (P) under RCP 8.5 [Colour figure can be viewed at wileyonlinelibrary.com]

those percentiles for a probabilistic assessment of climate change with a significance level of 0.05 ($\alpha = 0.05$).

To illustrate the temperature and precipitation changes at the tails of the distributions, the absolute values of the variables (temperature and precipitation) and the incremental differences (Δ in Figure 1b) between the distributions of the projection and baseline at 10% and 90% for temperature and precipitation are shown in Figure 5. The first column in Figure 5 shows temperature and precipitation at the tails of the projected distributions (corresponding to the 10th and 90th percentiles of the $ECDF_{Proj}$ in 2020–2049) and the second column shows the difference between projected and baseline distributions (Δ) at the 10th and 90th percentile under RCP 2.6.

Although the actual values of temperature at 10% are generally larger over the southwest/south of the domain, the difference between the distributions of the two periods (2020–2049 and 1976–2005) at 10% is more significant over the northeast (first row in Figure 5). This large difference indicates that the projected minimum temperatures increase relative to the minimum values in the baseline. For the 90th percentile, the larger actual values and the greater difference between the distributions of the temperature occur mainly in the southern part of the domain (second row in Figure 5). For precipitation, the minimum values (at 10%) increase mainly over the northern part of the domain (third row in Figure 5). Although many parts of the domain experience an increase in maximum values of precipitation (at 90%), the pattern of changes in precipitation at 90% is more complex than that at 10%. For instance, there are nearby pixels that experienced both an increase and a decrease in precipitation at 90% (fourth row in Figure 5). In addition, the projected extreme precipitation at 90% decreases mainly in southwest of the domain (e.g., Portugal and Spain). Note that differences between the distributions in the two periods (2020–2049 and 1976–2005) increase under RCP 8.5 (figure is not shown). Although the results concerning the extremes (Figures 3 and 5) can mainly be related to winter or summer, the lower (e.g., at 10%) and the upper (e.g., at 90%) end of the temperature distribution can be related to winter or fall and summer or spring as well, since climate change is also projected to affect these seasons (e.g., colder fall or warmer spring).

To evaluate climate change for different regions, four different subregions, namely East (G1), North (G2), West/South (G3), and UK/Ireland (G4), are considered (see Figure 6). The maximum increases in temperature

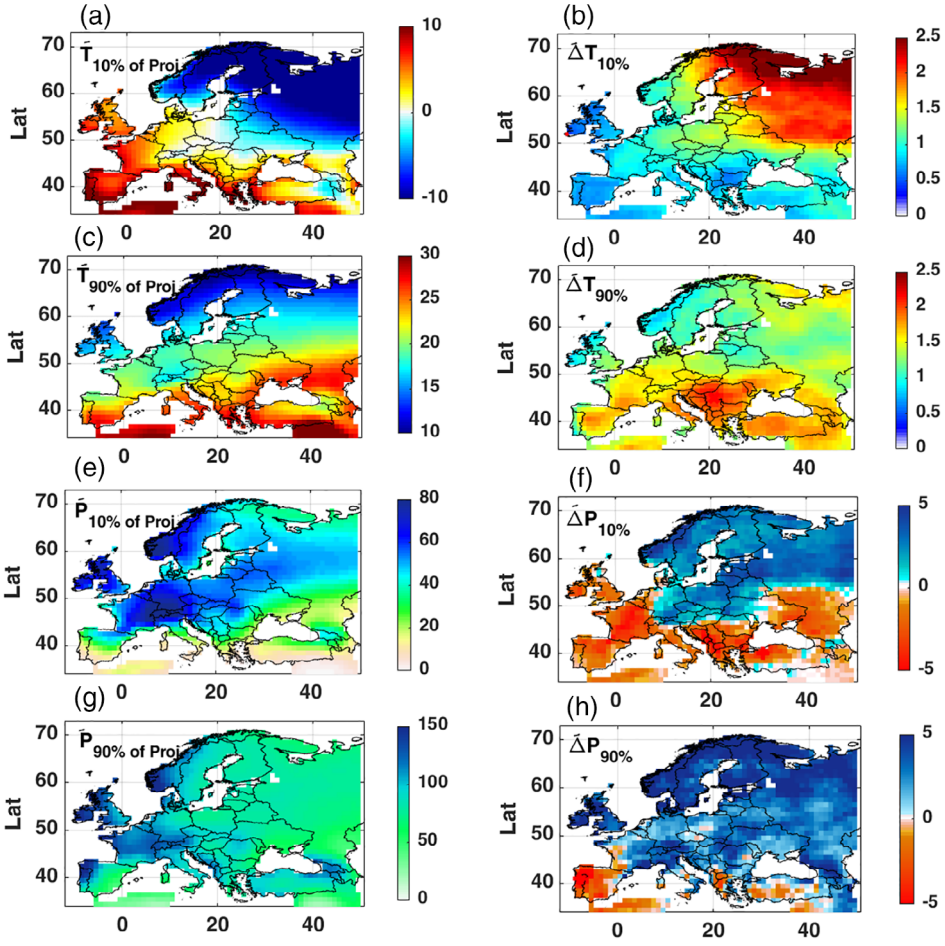

FIGURE 5 Extremes and their changes under RCP 2.6. Left column (from top to bottom): Temperature (°C) at 10% and 90% of the temperature distribution corresponding to each pixel in projection, precipitation ($mm \cdot Mon^{-1}$) at 10% and 90% of the precipitation distribution in projection. Right column: The difference between distributions of the two periods for (from top to bottom) temperature (°C) at 10% and 90%, precipitation ($mm \cdot Mon^{-1}$) at 10% and 90% (baseline: 1976–2005 and projection: 2020–2049) [Colour figure can be viewed at wileyonlinelibrary.com]

occur in G1, not only for the mean but also at extreme percentiles of the distribution. On the other hand, the maximum changes in precipitation, both in the mean and in extreme percentiles, occur in G4 and G2. Each region (pixel) can have the maximum changes between two periods at different quantiles. To illustrate quantiles that exhibit the largest change in each subregion, temperature and precipitation differences between the projection (2020–2049) and the historical (1976–2005) period are calculated (Δ) at median and extreme percentiles (50%, 10%, and 90%). The largest of the percentile-specific changes is then selected, and plotted in Figure 6 as "Max Δ".

This quantile analysis helps to illustrate the tendency of the regions towards wet/dry and hot/cold weather, which is useful information for adaptation and mitigation plans. Since this work attempts to highlight the extremes, dark colours including dark blue and dark pink in the second columns of Figure 6a and b show the 10th and 90th percentile, respectively. The light colours including light blue and light pink show small (e.g., 15th–25th) and large (e.g., 75th–85th) percentiles. Results show that the maximum difference between temperature distributions of the two periods (Max Δ in Figure 6) occurs in the northeast of the domain (in G1) at smaller percentiles (e.g., 10%). In general, regions above latitude 50°N in G1 experience the maximum difference at smaller extremes (dark blue colour in second column) and regions below 50°N experience the maximum difference at larger extremes (dark pink colour in second column). For G2,

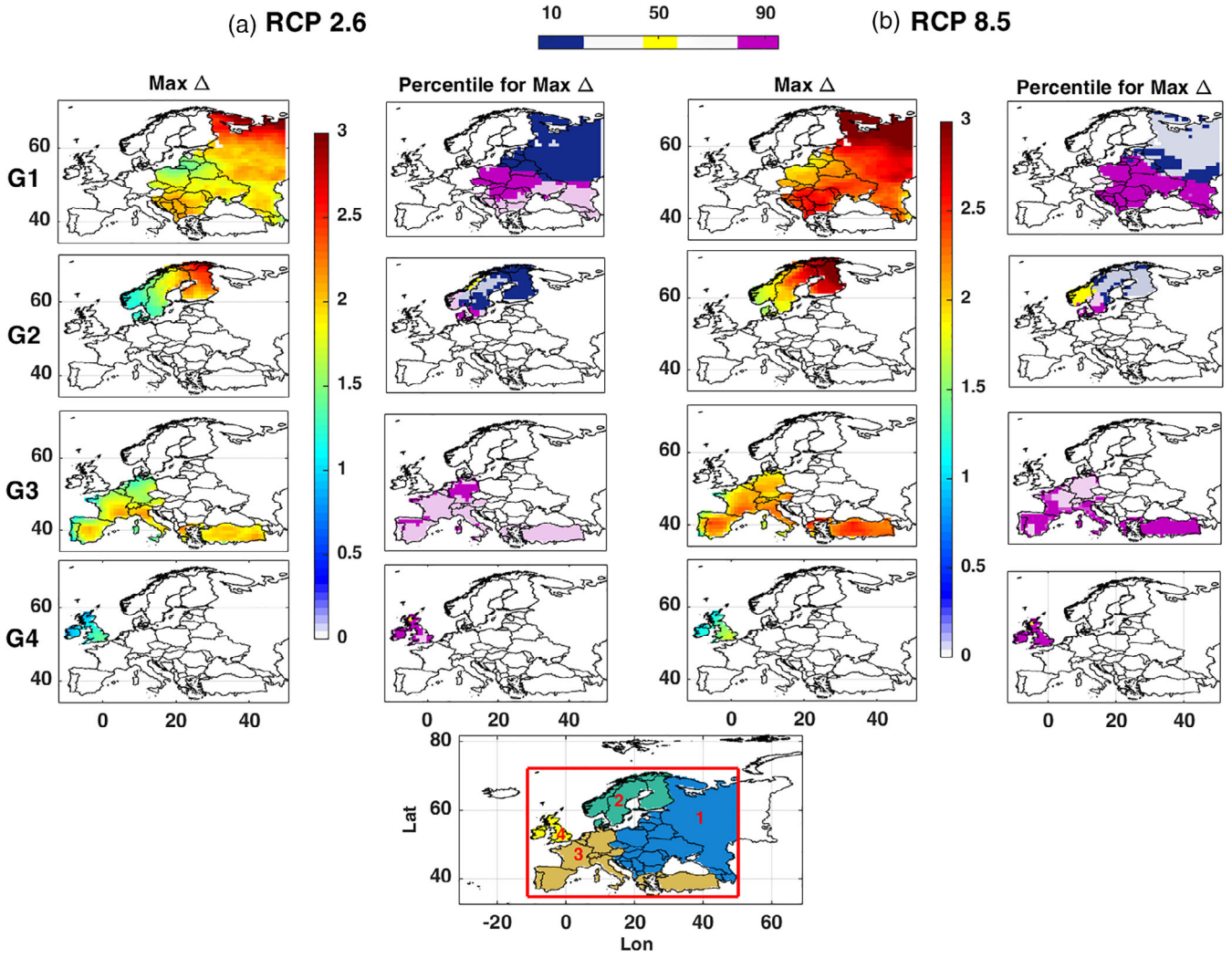

FIGURE 6 Maximum differences (max Δ) between projection (2020–2049) and historical (1976–2005) period at different percentiles including 10th, 50th, 90th percentiles (median and extremes) for temperature in four subregions. (top-bottom) subregions G1, G2, G3, and G4 in panel (a) for RCP 2.6 and panel (b) for RCP 8.5. Max Δ is shown in the first columns of the panels. The second columns of the panels show the percentiles (10%, 50%, and 90%, shown at top) at which "max Δ" occurs. Numbers 1, 2, 3, and 4 refer to four subregions (G1, G2, G3, and G4, respectively) [Colour figure can be viewed at wileyonlinelibrary.com]

most changes (Max Δ) occur at smaller extreme, while the maximum differences in G3 and G4 occur at larger extremes. For RCP 8.5, Max Δ not only increases in all subregions but also occurs generally at larger quantiles compared to those in RCP 2.6.

Similar to temperature, the pattern of percentile changes in precipitation for each subregion is illustrated in Figure 7.

Results illustrate that maximum differences (Max Δ) in the precipitation distribution mainly tend to occur at larger percentiles (second column), excluding small regions in G1, G2, and G3 (see the yellow and blue colour in the first, second, and third rows of the second column in Figure 7), where the maximum differences are more likely to occur at median and smaller percentiles. RCP 8.5 can cause both an increase in heavy precipitation and a decrease in light precipitation relative to RCP 2.6.

These results confirm that climate is projected to change and that to quantify these changes, measures, and indicators are required. Two measures of distribution changes, namely KS (see Equation 1) and Δ, are calculated for precipitation and temperature. The KS statistic applies to the projected (2020–2049) and historical (1976–2005) distributions on a pixel by pixel basis (Figure 8).

Figure 8 shows that on average the maximum KS (in terms of its absolute value) for temperature mainly occurs in the west and south of the domain. Negative values of KS indicate that the CDF of the projection is

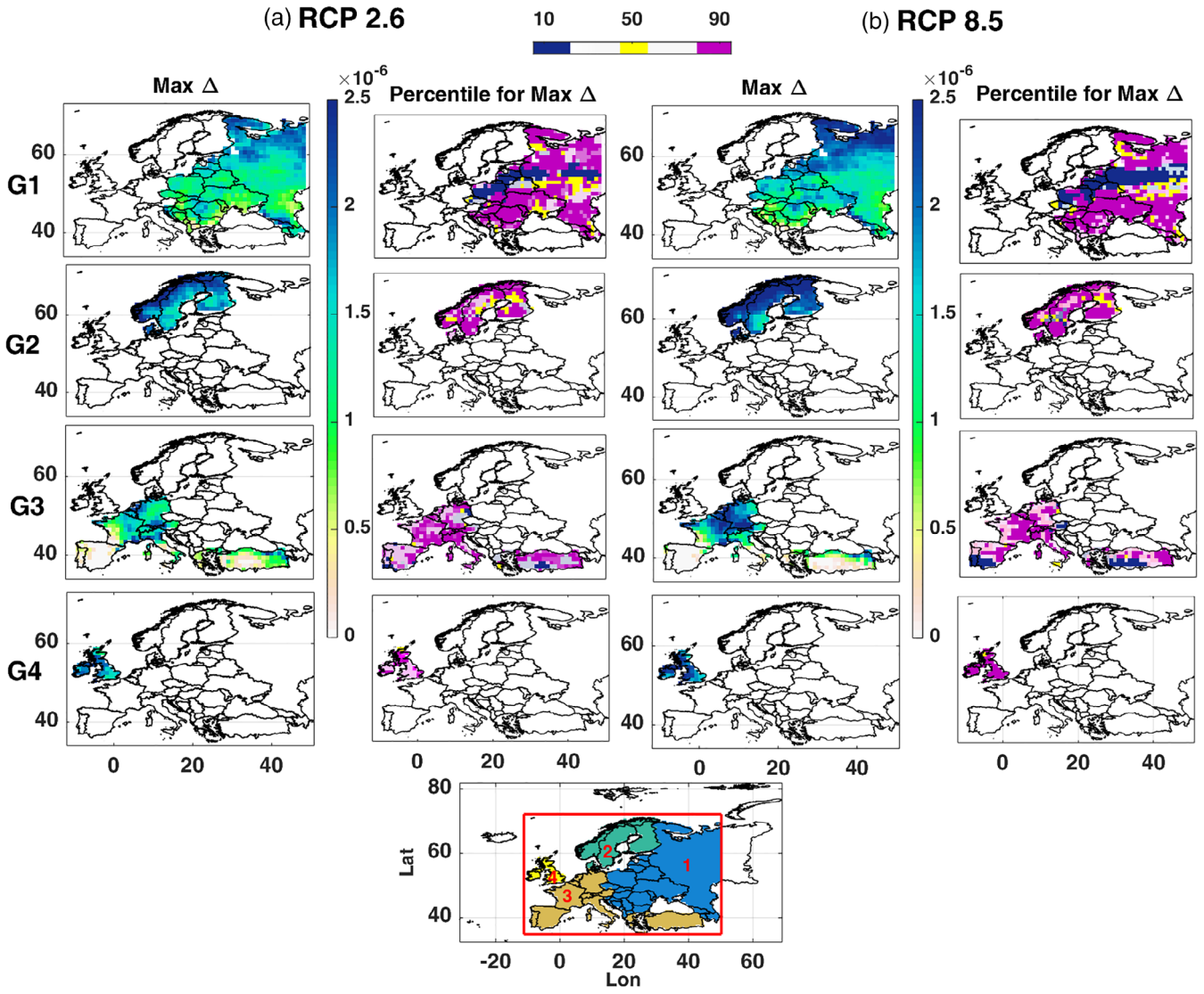

FIGURE 7 Maximum differences (max Δ) between projection (2020–2049) and historical (1976–2005) period at different percentiles including 10th, 50th, 90th percentiles (median and extremes) for precipitation in four subregions. (top-bottom) subregions G1, G2, G3, and G4 in panel (a) for RCP 2.6 and panel (b) for RCP 8.5. Max Δ is shown in the first columns of the panels. The second columns of the panels show the percentiles (10%, 50%, and 90%, shown at top) at which "max Δ" occurs. Numbers 1, 2, 3, and 4 refer to four subregions (G1, G2, G3, and G4, respectively) [Colour figure can be viewed at wileyonlinelibrary.com]

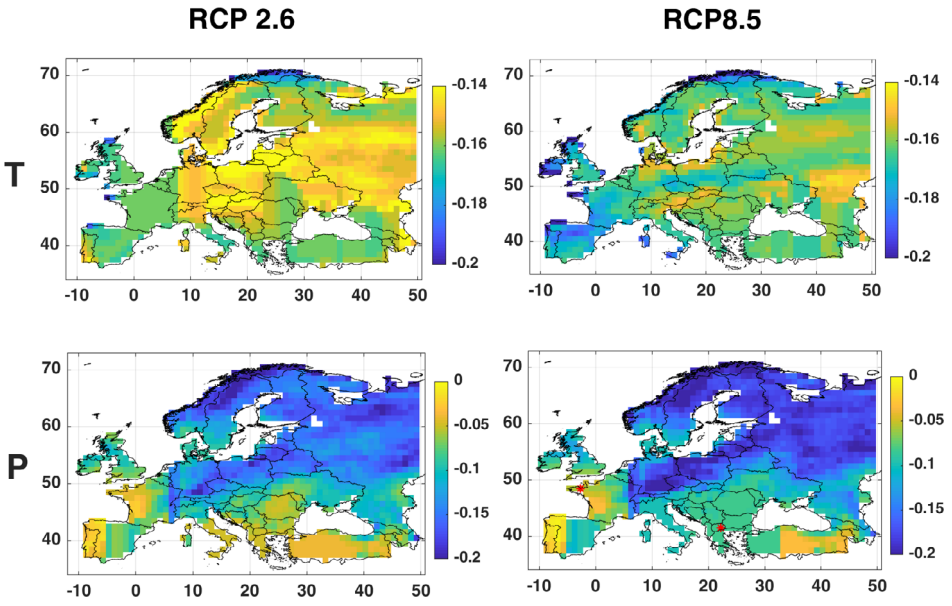

FIGURE 8 The largest vertical distances between projected and historical distributions (KS) for each pixel. (from top to bottom) Kolmogorov–Smirnov test statistic (KS) in temperature and precipitation under RCP 2.6 (left column) and RCP 8.5 (right column). Stars show pixels that are not statistically significant [Colour figure can be viewed at wileyonlinelibrary.com]

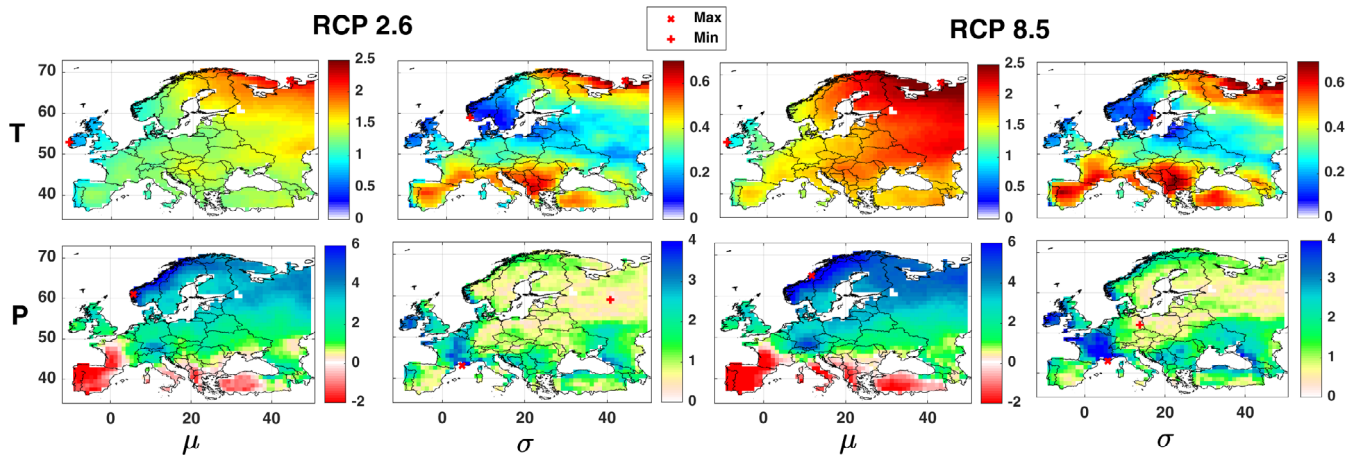

FIGURE 9 The mean (μ) and standard deviation (σ) of incremental differences (Δ) at different percentiles under RCP 2.6 and RCP 8.5 over the domain [Colour figure can be viewed at wileyonlinelibrary.com]

located below the CDF of the historical period. For precipitation, the maximum KS mainly occurs in the east and north of the domain, extending to the centre. In general, subregions G3 and G4 have the larger KS for temperature, while G1 and G2 have the larger KS values for precipitation. RCP 8.5 leads to increasing KS for both temperature and precipitation. For KS statistics, all pixels experience significant changes ($\alpha = 0.05$) excluding two pixels that are shown with the red star in Figure 8.

To assess the average and variability changes in the probability distributions of the projection compared to the historical baseline at different percentiles, the mean (μ) and standard deviation (σ) of the Δ at different percentiles is illustrated in Figure 9.

Figure 9 (μ in first row) shows that the average changes of temperature at different percentiles in most pixels of the domain are about 1.5°C and the maximum average changes occur over the northeast of the domain (about 2°C) for RCP2.6. These average changes of the temperature at different percentiles increase for RCP 8.5. The smallest average changes between the two distributions for the baseline and the projection at different percentiles occur in UK under both scenarios. The positive values of μ show that the distribution of the projection tends to be on the right-hand side of the historical distribution (e.g., larger values at extremes). The variability of the changes at different percentiles is larger in the northeast and south of the domain (σ in first row), which indicates that differences between the two distributions (baseline and projection) at different percentiles are spread out across a larger range. The average changes in precipitation at different percentiles are positive/negative

mainly above/below latitude 50°N for RCP 2.6 (μ in second row). The positive/negative values show that projected precipitation increases/decreases at different percentiles. The maximum average changes occur in the north of the domain. The absolute averages of the changes are larger for RCP 8.5, which can indicate that projected precipitation at different percentiles gets further away from the baseline precipitation. The variability of precipitation changes at different percentiles is larger in France, UK, and the southern parts of the domain for RCP 2.6 (σ in second row), which increases for RCP 8.5. The spatial pattern of precipitation differences between the two distributions (baseline and projection) is not as smooth as for temperature. This is a reflection of the complex and highly nonlinear process of precipitation, which is consistent with the results obtained by Moghim and Bras (2017, 2019).

6 | DISCUSSION AND CONCLUDING REMARKS

The impact of climate change on different moments of the distributions of the relevant climatological variables (i.e., temperature and precipitation) varies among different locations. To quantify these changes, appropriate measures and indicators are required. Indeed, different indices can provide different types of information and can indicate different levels of change. To evaluate historical and projected hydrometeorological changes, CRU and ensemble climate model datasets have been used. Since effects of climate change can vary between different percentiles (e.g., extremes), distribution changes at median and extremes (i.e., 50%, 10%, and 90%) have been calculated. The historical and projected assessment of climate change using CRU and ensemble data shows that, although temperature and precipitation averages have been increasing over Europe, the maximum differences between the distributions of the two historical and projection periods, generally, occur at the extremes (e.g., 10% and 90%).

Climate change and related studies include many uncertainties. To account for these, this study used a probability framework for the analysis. Results show that the probabilities of the occurrence of temperature extremes are increasing. The projected distribution is more likely to shift to larger temperatures. Results are consistent with the studies by Christidis *et al*., 2015 and Stott *et al*. (2016), which showed an increase in the probability of extreme temperature events since 2003. Increased temperature affected magnitude and frequency of the temperature-related extreme phenomena in Europe such as heat waves and wildfires (Stott *et al*., 2016; NASA, 2019), which caused a large number of deaths and severe losses (Schar and Jendtrizky, 2004; Stott *et al*., 2004; Kron *et al*., 2019; Weilnhammer *et al*., 2019). For precipitation, the largest extreme values (e.g., at the 90th percentile) are more likely to increase in many pixels of the domain. Results highlighted the non-uniform nature of climate change over different parts of the domain. IPCC (2014) also used a multi-model ensemble to show spatial heterogeneity of climate change. This variability and changes can be more notable in the future. The changes can be caused by the large-scale atmosphere–ocean circulation and multidecadal climate variability in the North Atlantic (O'Reilly *et al*., 2017). The impact of the Atlantic Multidecadal Oscillation (AMO) on the climate of Europe varies in different locations and seasons. For instance, the warm phase of the Atlantic Multidecadal Oscillation (AMO) in summer can lead to warmer temperatures and more precipitation in most parts of Europe and in the northwest of the continent, respectively (Knight *et al*., 2006). The warmer fall and spring seasons occur in northern and Western Europe, respectively (Sutton and Dong, 2012). Indeed, there can be seasonal contrasts in the temperature response, due to factors such as reduced westerly advection from sea to land in summer, the effects of drying soils (important in summer but not in winter), or albedo feedbacks (important in winter but not in summer).

Although spatial averages of temparature and precipitation show that climate has been changing, a pixel by pixel assessment of historical changes reveals that the central part of the study domain is more probable to experience precipitation extremes (i.e., Poland, Germany, Hungary, and Bulgaria) and the largest extreme temperatures (i.e., Ukraine, Hungary, Serbia, Croatia, and Austria). Similar to other studies (e.g., Pfeifer *et al*., 2019; Kjellström *et al*., 2018), our results confirmed that the largest increase in extreme temperature has mainly occurred over southern part of the study domain, while for precipitation large increases can be observed in different parts of the domain. Indeed, the maximum increase and decrease in extreme precipitation can occur at nearby pixels, which can confirm highly variabile precipitation events.

To assess climate change in the near future, temperature and precipitation outputs from an ensemble model projection under two scenarios (RCP 2.6 and RCP 8.5) are used. The average seasonal changes of the data show that, although temperature increases in summer nearly everywhere, the largest increase occurs in winter, which can affect the precipitation type (i.e., the snow-rain transition phase). Regions above (below) latitude 50°N can expect an increase (decrease) in precipitation particularly in summer. These changes are projected to be intensified

under RCP 8.5. Assessment of historical and projected climate change indicates that the largest changes in the precipitation and temperature distributions occur at larger (e.g., 90th) and smaller (e.g., 10th) percentiles. The increase of temperature over the northeast of the domain during the historical period extends to the east, centre, and north of Europe under RCP 2.6 and 8.5.

Greenhouse gas (GHG) emission is the main anthropogenic driver of climate change. The average CO_2 level during the baseline period (1976–2005) is 395 ppm, which on average increases with 98 and 172 ppm under RCP 2.6 and 8.5, respectively (Riahi *et al*., 2007; van Vuuren *et al*., 2007; Meinshausen *et al*., 2011). An increase of atmospheric CO_2 (e.g., in RCP 8.5) leads to a temperature rise, which can affect the magnitude and frequency of the extreme weather events. Results suggest that extreme weather events are closely tied to increasing rates of CO_2 emissions.

Climate change has different impacts depending on the region. Changes in temperature and precipitation distributions over four subregions within Europe, namely East (G1), North (G2), West/South (G3), and UK/Ireland (G4), are evaluated. Results revealed that the East of the study domain (G1) and UK/Ireland (G4) will experience the largest increases in extremes of temperature and precipitation, respectively. Indeed, the quantile evaluation provides valuable information for adaptation and mitigation plans to be prepared for possible effects of projected climate change such as floods and droughts (Kaspersen and Halsnæs, 2017; Tabari, 2021). Projected increased temperature in east and north of Europe and an increase in heavy precipitation is also shown by previous studies (Anders *et al*., 2014; Nolan *et al*., 2017). The maximum changes in temperature and precipitation in each subregion occur at different quantiles. For instance, the maximum temperature changes in East occur at smaller (larger) quantiles above (below) 50°N. Although the maximum changes of temperature occur at smaller quantiles in the north of the domain, regions in West/South (G3) and UK/Ireland (G4) experience the maximum changes at larger quantiles. In RCP 8.5, differences between projection and historical period increases particularly at larger quantiles, which can lead to more severe extremes. The maximum precipitation changes mainly occur at larger quantiles in all subregions, which indicates that the frequency of heavy rain events tends to increase.

A complete assessment and analysis of climate change need proper measures and indicators. To evaluate climate change at different percentiles, two indicators including the KS statistic and Δ are used to quantify changes based on differences between the projected distributions of precipitation and temperature (2020–2049) and the historical ones (1976–2005). The larger KS for temperature mainly occurs in west/south (G3) and UK/Ireland (G4), while east (G1) and north (G2) exhibit the larger KS in precipitation. The KS statistic increases under RCP 8.5. The Δ measure between the two distributions at different percentiles is used to calculate spatial mean and variability of the differences between future (2020–2049) and historical (1976–2005) distributions at different percentiles. Results show that the maximum variability (σ) for temperature Δ-values occurs over the west, south, and a small part in the north of the study domain, which can indicate the larger dispersion of these values at different percentiles around the mean. Although the projected temperatures are larger than the historical ones at different percentiles in all pixels, precipitation is projected to increase or decrease at different percentiles in different regions (positive or negative μ). The mean and variability of the projected temperature and precipitation increase under RCP 8.5, which can illustrate an intensification of the extreme events (e.g., strong floods or droughts). The larger mean of the Δ-values for RCP 8.5 occurs because the difference between the projected and historical distributions is greater than that for RCP 2.6. The large spatial variability of the precipitation can reflect the highly nonlinear process of precipitation, with a high level of uncertainty. These indicators can illustrate different aspects of the projected changes in the distribution of the climatological variables (temperature and precipitation). Note that biases in the climate model influence the results. In addition, different scenarios (RCPs) can affect the extremes values in temperature and precipitation. The probability framework and indicators can be used for multi-models to show projected ranges of the extremes and changes at different percentiles.

Climate change affects magnitude and variability of the climatological variables at different quantiles and boosts extreme weather events (i.e., droughts, wildfires, heavy rains, and floods). A complete assessment and proper statistical measures can provide valuable overview and insights, which are required for adaptation and mitigation plans. Since future is uncertain, we need to consider a wide range of possible changes in order to reduce damage and losses. Analysis of projected changes in the probabilistic framework is crucial for impact assessment and risk management.

ACKNOWLEDGEMENTS

The authors would like to thank climate modellers that make their datasets and documents publicly available. The data used in this study were provided by the Climate Research Unit, University of East Anglia (UK) and modelling groups involved in preparing the Coupled

Model Intercomparison Project Phase 5 (CMIP5) multi-model ensemble. We recognize Dr. Jean-Francois Lamarque for his suggestions in this paper. Hospitality and support by Wageningen University & Research during this work is also gratefully acknowledged.

AUTHOR CONTRIBUTIONS

Sanaz Moghim: Conceptualization; data curation; formal analysis; investigation; methodology; validation; visualization; writing – original draft; writing – review and editing. **Adriaan J Teuling:** Conceptualization; methodology; writing – review and editing. **Remko Uijlenhoet:** Conceptualization; methodology; writing – review and editing.

ORCID

Sanaz Moghim https://orcid.org/0000-0002-6320-1374
Adriaan J. Teuling https://orcid.org/0000-0003-4302-2835
Remko Uijlenhoet https://orcid.org/0000-0001-7418-4445

REFERENCES

Alexander, L.V. and Arblaster, J.M. (2017) Historical and projected trends in temperature and precipitation extremes in Australia in observations and CMIP5. *Weather and Climate Extremes*, 15, 34–56.

Anders, I., Stagl, J., Auer, I. and Pavlik, D. (2014) Climate change in central and Eastern Europe. In: Rannow, S. and Neubert, M. (Eds.) *Managing protected areas in central and eastern Europe under climate change, advances in global change research*, Vol. 58. Dordrecht: Springer.

Blöschl, G., Hall, J., Viglione, A., Perdigão, R.A.P., Parajka, J., Merz, B., Lun, D., Arheimer, B., Aronica, G.T., Bilibashi, A., Boháč, M., Bonacci, O., Borga, M., Čanjevac, I., Castellarin, A., Chirico, G.B., Claps, P., Frolova, N., Ganora, D., Gorbachova, L., Gül, A., Hannaford, J., Harrigan, S., Kireeva, M., Kiss, A., Kjeldsen, T.R., Kohnová, S., Koskela, J.J., Ledvinka, O., Macdonald, N., Mavrova-Guirguinova, M., Mediero, L., Merz, R., Molnar, P., Montanari, A., Murphy, C., Osuch, M., Ovcharuk, V., Radevski, I., Salinas, J.L., Sauquet, E., Šraj, M., Szolgay, J., Volpi, E., Wilson, D., Zaimi, K. and Živković, N. (2019) Changing climate both increases and decreases European river floods. *Nature*, 573, 108–111. https://doi.org/10.1038/s41586-019-1495-6.

Casanueva, A., Rodríguez-Puebla, C., Frías, M.D. and González-Reviriego, N. (2014) Variability of extreme precipitation over Europe and its relationships with teleconnection patterns. *Hydrology and Earth System Sciences*, 18, 709–725.

Christidis, N., Jones, G.S. and Stott, P.A. (2015) Dramatically increasing chance of extremely hot summers since the 2003 European heatwave. *Nature Climate Change*, 5, 46–50.

Climate Change Index. (2013), International Geosphere-Biosphere Programs (IGBP), Retrieved from http://www.igbp.net/globalchange

Cohen, J., Ye, H. and Jones, J. (2015) Trends and variability in rain-on-snow events. *Geophysical Research Letters*, 42, 7115–7122.

Collins, M., Knutti, R., Arblaster, Dufresne, J.-L., Fichefet, T., Friedlingstein, P., Gao, X., Gutowski, W.J., Johns, T., Krinner, G., Shongwe, M., Tebaldi, C., Weaver, A.J. and Wehner, M. (2013) Long-term climate change: projections, commitments and irreversibility. In: Stocker, T.F., Qin, D., Plattner, G.-K., Tignor, M., Allen, S.K., Boschung, J., Nauels, A., Xia, Y., Bex, V. and Midgley, P.M. (Eds.) *Climate Change 2013: The Physical Science Basis. Contribution of Working Group I to the Fifth Assessment Report of the Intergovernmental Panel on Climate Change*. Cambridge, United Kingdom and New York, NY, USA: Cambridge University Press.

Dessai, S., Lu, X. and Hulme, M. (2005) Limited sensitivity analysis of regional climate change probabilities for the 21st century. *Journal of Geophysical Research*, 110, D19.

Dhakal, N. and Tharu, B. (2018) Spatio-temporal trends in daily precipitation extremes and their connection with North Atlantic tropical cyclones for the southeastern United States. *International Journal of Climatology*, 38, 3822–3831.

Dosio, A. (2017) Projection of temperature and heat waves for Africa with an ensemble of CORDEX regional climate models. *Climate Dynamics*, 49, 493–519.

Ganguli, P. and Ganguly, A.R. (2016) Space-time trends in U.S. meteorological droughts. *J. Hydrology: Regional Studies*, 8, 235–259.

Harris, I., Jones, P.D., Osborn, T.J. and Lister, D.H. (2014) Updated high-resolution grids of monthly climatic observations the CRU TS3.10 dataset. *International Journal of Climatology*, 34, 623–642.

IPCC. (2007) *The Physical Science Basis.Contribution ofWorking Group I to the Fourth Assessment Report of the Intergovernmental Panel on Climate Change [Solomon, S., D. Qin, M. Manning, M. Marquis, K. Averyt, M.M.B. Tignor, H.L. Miller Jr., and Z. Chen (eds)]*. Cambridge, UK and New York, NY, USA: Cambridge University Press, p. 996.

IPCC. (2014) *Climate Change 2014: Synthesis Report. Contribution of Working Groups I, II and III to the Fifth Assessment Report of the Intergovernmental Panel on Climate Change [Core Writing Team, R.K. Pachauri and L.A. Meyer (eds.)]*. Geneva, Switzerland: IPCC, p. 151.

Jacob, D., Petersen, J., Eggert, B., Alias, A., Christensen, O.B., Bouwer, L.M., Braun, A., Colette, A., Déqué, M., Georgievski, G., Georgopoulou, E., Gobiet, A., Menut, L., Nikulin, G., Haensler, A., Hempelmann, N., Jones, C., Keuler, K., Kovats, S., Kröner, N., Kotlarski, S., Kriegsmann, A., Martin, E., van Meijgaard, E., Moseley, C., Pfeifer, S., Preuschmann, S., Radermacher, C., Radtke, K., Rechid, D., Rounsevell, M., Samuelsson, P., Somot, S., Soussana, J.F., Teichmann, C., Valentini, R., Vautard, R., Weber, B. and Yiou, P. (2014) EURO-CORDEX: new high-resolution climate change projections for European impact research. *Regional Environmental Change*, 14, 563–578.

Jahangir, M.S. and Moghim, S. (2019) Assessment of the urban heat Island in the city of Tehran using reliability methods. *Atmospheric Research*, 225, 144–156.

Jeong, D.I., Sushama, L., Diro, G.T., Khaliq, M.N., Beltrami, H. and Caya, D. (2016) Projected changes to high temperature events for Canada based on a regional climate model ensemble. *Climate Dynamics*, 46, 3163–3180.

Karl, T.R., Meehl, G.A., Miller, C.D., Hassol, S. J., Waple, A.M., Murray, W.L., Eds. (2008) Weather and climate extremes in a

changing climate. Regions of focus: North America, Hawaii, Caribbean, and U.S. Pacific Islands. Department of Commerce, NOAA's National Climatic Data Center, 164 pp.

Kaspersen, P.S. and Halsnæs, K. (2017) Integrated climate change risk assessment: a practical application for urban flooding during extreme precipitation. *Climate Services*, 6, 55–64.

Kew, S.F., Philip, S.Y., van Oldenborgh, G.J., Otto, F.F.L., Vautard, R. and van der Schrier, G. (2019) The exceptional summer heat wave in southern Europe 2017 [in "explaining extremes of 2017 from a climate perspective"]. *Bull. Amer. Meteor. Soc.*, 100, S111–S117.

Kjellström, E., Nikulin, G., Strandberg, G., Christensen, O.B., Jacob, D., Keuler, K., Lenderink, G., van Meijgaard, E., Schär, C., Somot, S., Sørland, S.L., Teichmann, C. and Vautard, R. (2018) European climate change at global mean temperature increases of 1.5 and 2 °C above pre-industrial conditions as simulated by the EURO-CORDEX regional climate models. *Earth System Dynamics*, 9, 459–478.

Knight, J.R., Folland, C.K. and Scaife, A.A. (2006) Climate impacts of the Atlantic multidecadal oscillation. *Geophysical Research Letters*, 33, L17706.

Koenker, R. (2005) Frontmatter. In: *Quantile Regression (Econometric Society Monographs, pp. I–VI)*. Cambridge: Cambridge University Press.

Kossin, J.P. (2018) A global slowdown of tropical-cyclone translation speed. *Nature*, 558, 104–107.

Kron, W., Löwa, P. and Kundzewicz, Z.W. (2019) Changes in risk of extreme weather events in Europe. *Environmental Science & Policy*, 100, 74–83.

Lausier, A.M. and Jain, S. (2018) Overlooked trends in observed global annual precipitation reveal underestimated risks. *Scientific Reports*, 8, 16746.

Lhotka, O., Kyselý, J. and Farda, A. (2018) Climate change scenarios of heat waves in Central Europe and their uncertainties. *Theoretical and Applied Climatology*, 131, 1043–1054.

Li, H., Sheffield, J. and Wood, E.F. (2010) Bias correction of monthly precipitation and temperature fields from intergovernmental panel on climate change AR4 models using equidistant quantile matching. *Journal of Geophysical Research*, 115, D10101.

Meinshausen, M., Smith, S., et al. (2011) The RCP greenhouse gas concentrations and their extension from 1765 to 2500. *Climatic Change (Special Issue on RCPs)*, 109, 213–241.

Min, E., Hazeleger, W., van Oldenborgh, G.J. and Sterl, A. (2013) Evaluation of trends in high temperature extremes in North-Western Europe in regional climate models. *Environmental Research Letters*, 8, 014011.

Moghim, S. (2018) Impact of climate change on hydrometeorology in Iran. *J. Glob. Planet. Change*, 170, 93–105.

Moghim, S. (2021) Reliability assessment of the wind power density using uncertainty analysis. *Sustain. Energy Technol. Assess.*, 44, 100964.

Moghim, S. and Bras, R.L. (2017) Bias correction of climate modeled temperature and precipitation using artificial neural networks. *Journal of Hydrometeorology*, 18, 1867–1884.

Moghim, S. and Bras, R.L. (2019) Regression-based regionalization for bias correction of temperature and precipitation. *International Journal of Climatology*, 39, 3298–3312.

Moghim, S., McKnight, S.L., Zhang, K., Ebtehaj, A.M., Knox, R.G., Bras, R.L., Moorcroft, P.R. and Wang, J. (2016) Bias-corrected data sets of climate model outputs at uniform space time resolution for land surface modeling over Amazonia. *International Journal of Climatology*, 37, 621–636.

Moon, I., Kim, S. and Chan, J.C.L. (2019) Climate change and tropical cyclone trend. *Nature*, 570, E3–E5.

Moss, R., et al. (2008) *Towards new scenarios for analysis of emissions, climate change, impacts, and response strategies*. Geneva: Intergovernmental Panel on Climate Change, p. 132.

Moss, R.H. (2010) The next generation of scenarios for climate change research and assessment. *Nature*, 463, 747–756.

Nakicenovic, N., Davidson, O., Davis, G., Grübler, A., Kram, T., Rovere, E. L. L., Metz, B., Morita, T., Pepper, W., Pitcher, H., Sankovski, A., Shukla, P., Swart, R., Watson, R., Dadi, Z. (2000) Emissions Scenarios. A Special Report of Working Group III of the Intergovernmental Panel on Climate Change, IPCC [Summary for Policymakers].

NASA. 2019, Global Climate Change, Vital signs of the planet. Retrieved from https://climate.nasa.gov/news/2865/a-degree-of-concern-why-global-temperatures-matter

Nolan, P., O'Sullivan, J. and McGrath, R. (2017) Impacts of climate change on mid-twenty-first-century rainfall in Ireland: a high-resolution regional climate model ensemble approach. *International Journal of Climatology*, 37, 4347–4363.

O'Reilly, C.H., Woollings, T. and Zanna, L. (2017) The dynamical influence of the Atlantic multidecadal oscillation on continental climate. *Journal of Climate*, 30, 7213–7230.

Pfeifer, S., Rechid, D., Reuter, M., Viktor, E. and Jacob, D. (2019) 1.5°, 2°, and 3° global warming: visualizing European regions affected by multiple changes. *Regional Environmental Change*, 19, 1777–1786.

Philip, S., Sparrow, S., Kew, S.F., van der Wiel, K., Wanders, N., Singh, R., Hassan, A., Mohammed, K., Javid, H., Haustein, K., Otto, F.E.L., Hirpa, F., Rimi, R.H., Islam, A.K.M.S., Wallom, D.C.H. and van Oldenborgh, G.J. (2019) Attributing the 2017 Bangladesh floods from meteorological and hydrological perspectives. *Hydrology and Earth System Sciences*, 23, 1409–1429.

Philip, S.Y., Kew, S.F., Hauser, M., Guillod, B.P., Teuling, A.J., Whan, K., Uhe, P. and Oldenborgh, G.J.. (2018) Western US high June 2015 temperatures and their relation to global warming and soil moisture. *Climate Dynamics*, 50, 2587–2601.

Riahi, K., Gruebler, A. and Nakicenovic, N. (2007) Scenarios of long-term socio-economic and environmental development under climate stabilization. *Technological Forecasting and Social Change*, 74(7), 887–935.

Richardson, D., Neal, R., Dankers, R., Mylne, K., Cowling, R., Clements, H. and Millard, J. (2020) Linking weather patterns to regional extreme precipitation for highlighting potential flood events in medium- to long-range forecasts. *Meteorological Applications*, 27, e1931.

Schar, C. and Jendtrizky, G. (2004) Hot news from summer 2003. *Nature*, 432, 559–560.

Sheffield, J., Goteti, G. and Wood, E.F. (2006) Development of a 50-year high-resolution global dataset of meteorological forcings for land surface modeling. *Journal of Climate*, 19, 3088–3111.

Sheikh, M.M., Manzoor, N., Ashraf, J., Adnan, M., Collins, D., Hameed, S., Manton, M.J., Ahmed, A.U., Baidya, S.K., Borgaonkar, H.P., Islam, N., Jayasinghearachchi, D., Kothawale, D.R., Premalal, K.H.M.S., Revadekar, J.V. and

Shrestha, M.L. (2015) Trends in extreme daily rainfall and temperature indices over South Asia. *International Journal of Climatology*, 35, 1625–1637.

Sippel, S., Otto, F.E.L., Flach, M. and van Oldenborgh, G.J. (2016) The role of anthropogenic warming in 2015 central European heat waves [in "explaining extreme events of 2015"]. *Bull. Amer. Meteor. Soc.*, 97, S51–S56.

Solomon, S., et al. (2007) *Climate Change 2007—The Physical Science Basis*. Cambridge, U.K., and New York: Cambridge University Press, p. 996.

Stott, P. (2016) How climate change affects extreme weather events. *Science*, 352, 1517–1518.

Stott, P.A., Christidis, N., Otto, F.E.L., Sun, Y., Vanderlinden, J.P., van Oldenborgh, G.J., Vautard, R., von Storch, H., Walton, P., Yiou, P. and Zwiers, F.W. (2016) Attribution of extreme weather and climate-related events. *WIREs Climate Change*, 7, 23–41.

Stott, P.A., Stone, D.A. and Allen, M.R. (2004) Human contribution to the European heatwave of 2003. *Nature*, 432, 610–614.

Sutton, R.T. and Dong, B. (2012) Atlantic Ocean influence on a shift in European climate in the 1990s. *Nature Geoscience*, 5, 788–792.

Tabari, H. (2021) Extreme value analysis dilemma for climate change impact assessment on global flood and extreme precipitation. *Journal of Hydrology*, 593, 125932.

Teuling, A.J. (2018) A hot future for European droughts. *Nature Clim Change*, 8, 364–365.

Teuling, A.J., de Badts, E.A.G., Jansen, F.A., Fuchs, R., Buitink, J., Hoek van Dijke, A.J. and Sterling, S.M. (2019) Climate change, reforestation/afforestation, and urbanization impacts on evapotranspiration and streamflow in Europe. *Hydrology and Earth System Sciences*, 23, 3631–3652.

van den Besselaar, E.J.M., Klein Tank, A.M.G. and Buishand, T.A. (2013) Trends in European precipitation extremes over 1951–2010. *International Journal of Climatology*, 33, 2682–2689.

van der Schrier, G., Besselaar, E.J.M., Klein Tank, A.M.G. and Verver, G. (2013) Monitoring European average temperature based on the E-OBS gridded data set. *Journal of Geophysical Research*, 118, 5120–5135.

van der Wiel, K., Kapnick, S.B., van Oldenborgh, G.J., Whan, K., Philip, S., Vecchi, G.A., Singh, R.K., Arrighi, J. and Cullen, H. (2017) Rapid attribution of the august 2016 flood-inducing extreme precipitation in South Louisiana to climate change. *Hydrology and Earth System Sciences*, 21, 897–921.

van Vuuren, D., den Elzen, M., Lucas, P., Eickhout, B., Strengers, B., van Ruijven, B., Wonink, S. and van Houdt, R. (2007) Stabilizing greenhouse gas concentrations at low levels: an assessment of reduction strategies and costs. *Climatic Change*, 81, 119–159.

Watterson, I.G. (2008) Calculation of probability density functions for temperature and precipitation change under global warming. *Journal of Geophysical Research*, 113, D12.

Weilnhammer, V., Jiang, L., Pastuhovic, V., Weber, A., Heinze, S. and Herr, C. (2019) Extreme weather events in Europe and their possible health consequences; a systematic review. *Environmental Epidemiology*, 3, 432–433. https://doi.org/10.1097/01.EE9.0000610864.22562.5a.

Witze, A. (2019) Dramatic Sea-ice melt caps tough Arctic summer. *Nature*, 573, 320–321.

WMO. (2019) The Global Climate in 2015–2019, World Meteorological Organization (WMO). Retrieved from: https://library.wmo.int/index.php?lvl=notice_display&id=21522#.XcAiza-_OM9

Wu, J., Gao, X., Giorgi, F. and Chen, D. (2017) Changes of effective temperature and cold/hot days in late decades over China based on a high resolution gridded observation dataset. *International Journal of Climatology*, 37, 788–800.

Ye, H. and Cohen, J. (2013) Shorter snowfall season associated with higher air temperatures over northern Eurasia. *Environ. Res. Lett.*, 8, 014.

How to cite this article: Moghim, S., Teuling, A. J., & Uijlenhoet, R. (2022). A probabilistic climate change assessment for Europe. *International Journal of Climatology*, 1–17. https://doi.org/10.1002/joc.7604